J. Biomechanics, Vol. 3, pp. 495–511. Pergamon Press, 1970. Printed in Great Britain

MECHANICAL PROPERTIES OF CRANIAL BONE*

JAMES H. McELHANEY, JOHN L. FOGLE,† JOHN W. MELVIN,
RUSSELL R. HAYNES,† VERNE L. ROBERTS and NABIH M. ALEM†
Highway Safety Research Institute, The University of Michigan, Ann Arbor, Mich. 48105, U.S.A.

Abstract – Samples of human and *Macaca mulatta* cranial bone have been tested quasistatically in tension, compression, simple shear, and torsion. The results of these experiments have been analyzed, taking into account observed anisotrophies and varying structures. Statistical correlations of properties have been made with density and a model proposed that summarizes these results. The cranial bones appear to be transversely isotropic and they are generally much stronger and stiffer in the transverse or tangent to the skull direction in comparison to the radial direction. The structure of the diploë region was found to be highly variable and this strongly influenced many of the mechanical responses. The model, however, explains much of the observed variation.

INTRODUCTION

WITH the advent of high speed air and land transportation, engineers have become increasingly aware of the mechanical frangibility of the human body. Thus, we have seen the evolution of various isolating and load distributing devices ranging from seat belts and padded sun visors to ejection seats, crash helmets and acceleration couches. While there is much information available regarding the response of inanimate material to vibration and impact, there is an equal dearth of knowledge pertaining to the mechanical properties of biological materials. Therefore, the design of much support equipment is often based on intuition because of this lack of information. Knowledge of this type is valuable in the treatment of injuries since it serves to identify the mechanism of trauma. A rational therapy for head injury, for example, cannot be developed until a quantitative description of the mechanical properties of the tissues of the head is obtained.

The National Safety Council has shown that accidents are the fourth leading cause of death surpassed only by heart disease, cancer and stroke. Head injury ranks as a major cause of death and disability in this country (Subcommittee on Head Injury, 1969), with an estimate that head injuries occur in 71 per cent of persons injured in motorcycle accidents and in 70 per cent of persons injured in accidental falls in the home. It is further estimated that in 1967 there were 112,000 fatalities and 400,000 permanent impairments due to accidental causes. While data is not available as to what proportion of these were head injuries, there is little doubt that the percentage is discouragingly high.

The literature on the mechanical properties of the skull is quite modest. Evans and Lissner (1957) have measured the tensile and compressive strength of embalmed human parietal bone but they have not measured strains during the test and therefore could not report the modulus of elasticity. Dempster (1967) has made a detailed study of the cortical grain structure of the human skull using the split line method. He observed a random orientation of grain structure for the inner and outer table of the brain case, supporting our observation of isotropy in the tangential direction for skull bone. Wood (1969) recently finished a detailed study of the tensile properties of

*Received 31 March 1970.
†Biomechanics Laboratory, West Virginia University, Morgantown, W.V. 26505, U.S.A.

miniature specimens cut from the compact bone of the inner and outer tables while Melvin *et al.* (1969) has presented a preliminary report on the mechanical behavior of the diploë layer in compression.

The aim of the research described in this paper is to specify the mechanical properties of the skull relevant to the biomechanics of head injury. This work is part of a program of head injury research investigating the mechanical properties of all the tissues of the head. The ultimate goal of this program is to determine the characteristics of these materials in sufficient detail so that appropriate physical and mathematical models of the head may be constructed. These models will allow the systematic study of various head injury mechanisms.

The skull is a complex structure made up of several bones each with its own unique internal and external geometry. Mechanical properties may be classified in three types: geometrical or spatial properties; material properties; and structural properties. The measurement of all types of mechanical properties will be discussed in this paper. Each category presents its own peculiar measurement problems and it is important to separate these measurements as to type. In particular, material properties should be separated from structural properties. For instance, load deflection curves may be easily measured on a variety of structures and are in general as much property of the structure as of the material of which the structure is composed. It is only under certain highly restrictive conditions that such curves may be converted to stress–strain curves or material properties that are independent of the structural geometry. The stress and strain distributions must be known. It is possible to measure material properties in tension or compression tests by assuming and insuring that the stress and strain are uniformly distributed. This can only be completely true if the material under test is homogeneous. A beam or simple shear test requires a knowledge of the materials' stress–strain relations for interpretation and therefore yields only composite structural-material properties that cannot be uncoupled without additional information about the material (Gurdjian and Lissner, 1947). In the case of the small samples of skull bone it is convenient to consider the specimen homogeneous because the internal architecture cannot be determined in sufficient detail to allow a geometrical or structural analysis. Thus, the average stress and strain may be computed from the load, deformation, and the gross dimensions of the specimen. But the average value may be far from the maximum value because of the non-homogeneous microstructure (Evans and Bang, 1967). It is beyond the scope of this paper to deal with the influence of various levels of organization of bone on the stress distribution. Therefore, average values of stress and strain are reported throughout. However, the model presented here provides some insight into these problems and hopefully will allow the use of these average values in a more general way.

SPECIMEN PREPARATION AND LOCATION

The human skull bone used in this research was obtained from three sources: embalmed cadavers, craniotomies and autopsy. The primary source was embalmed cadavers from which 17 entire calvariums have been obtained with ages ranging from 56 to 73 yr at death. Fresh material from craniotomies and autopsy was also tested (40 donors) to verify the results of the tests on embalmed material. Previous work (McElhaney *et al.*, 1964) indicates that the mechanical properties of embalmed bone are not significantly different from immediate postmortem properties.

A fine grid reference system was used to identify the location of test specimens from the human and monkey skull. The system used a 1 cm grid referenced from the coronal, sagittal and lambdoidal sutures and originating from the bregma and lambda points. The system is based entirely on the landmarks on the top of the skull and has been used in an

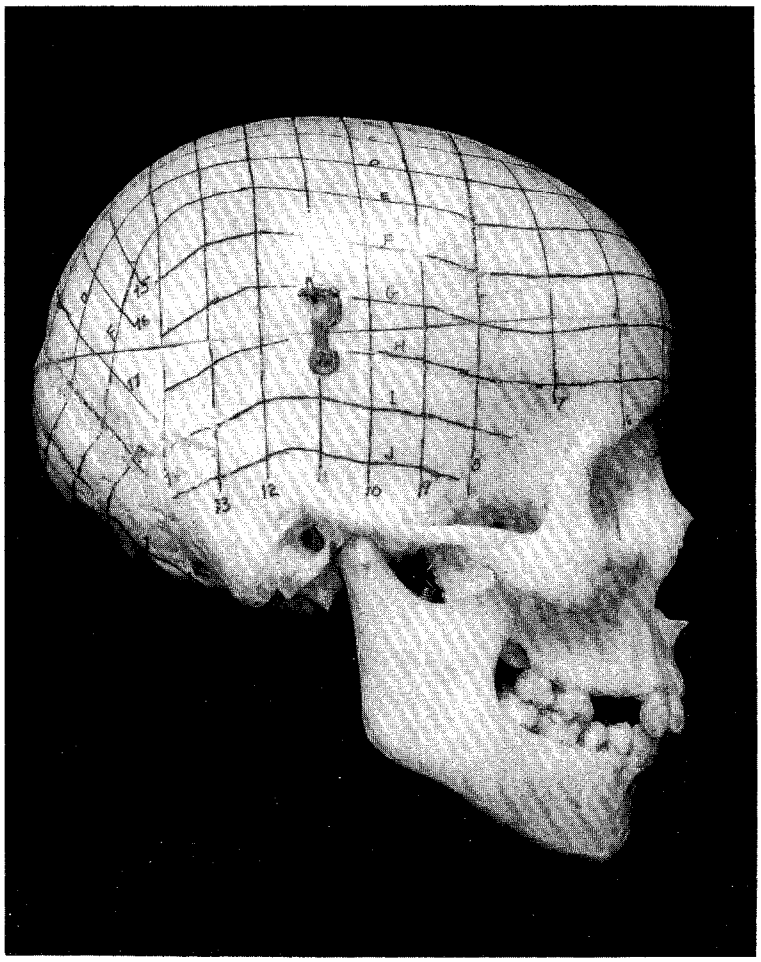

Fig. 1. Grid reference system.

(*facing p.* 496)

attempt to correlate the mechanical properties with position (Fig. 1).

Three types of specimens were prepared from human skull bone. Specimen type 'A' was a 10-mm dia. cylinder prepared by coring the skull with a Stryker oscillating core saw. Water was applied to the saw during cutting to prevent excessive heating. The thickness 't' was the skull thickness. These specimens are used in simple shear and torsion tests.

Specimen type 'B' was prepared from a 10-mm core. Specially designed fixtures with micrometer drives were used to precisely grind a cuboidal shape with parallel surfaces. All machining was done wet to avoid excessive heating of the specimen. These specimens were used in the triaxial compression tests.

Specimen type 'C' was a reduced section tension specimen produced by grinding a reasonably flat slice of bone between steel templates. Because of the parallel side requirement only a few specimens of this type could be made from each skull.

Only one type of monkey specimen had been used because of the extreme thickness of the monkey skull. This specimen was a curved flap cut from the skull and ground flat and parallel on the edges. It was used for compression tests in the tangential to the skull directions. Figure 2 shows the shape and dimensions of these specimens. After preparation, the specimens were kept damp with isotonic saline buffered with calcium. All tests were made on bone in a moist condition.

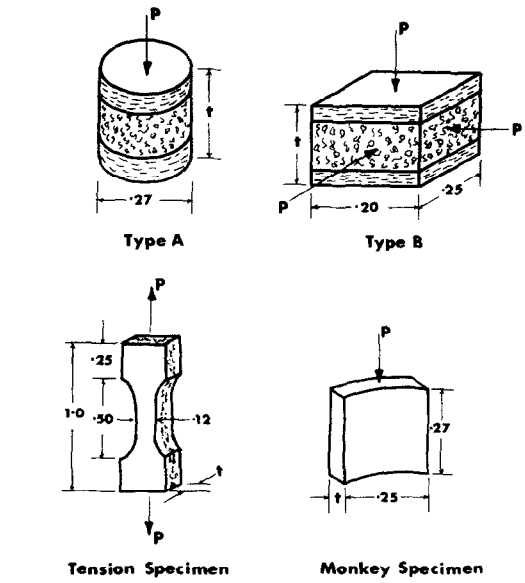

Fig. 2. Specimen types and sizes.

STRUCTURE AND GEOMETRY

The skull bones considered here were the frontal, right and left parietal, and the occipital. Figure 3 compares a section through the right and left parietal of the human with the Rhesus monkey (*Macaca mulatta*). In the human, these bones show a well-defined shell of compact bone separated by a core of spongy cancellous bone (diploë). Compact bone surrounds and reinforces the sutures. The thickness of the spongy core increases toward the center of the bone away from the sutures.

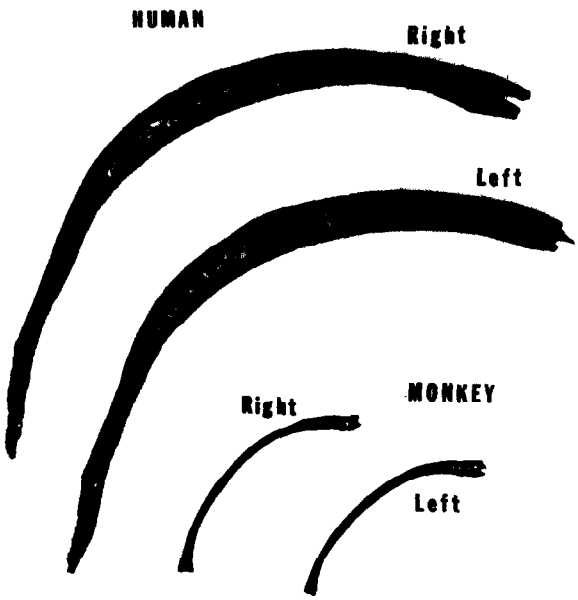

Fig. 3. Sections through human and primate (*Macaca mulatta*) parietal bone.

The spongy bone is quite variable in structure with marrow spaces normally ranging from 3-mm dia. down to microscopic size. The outer

table of compact bone is quite smooth. The inner surface presents depressions corresponding to the cerebral convolutions, and numerous furrows for the ramifications of various blood vessels. The structure of these bones in the Rhesus monkey is quite different from the human for there is much less diploë and where it occurs it is generally one to two pores thick.

Due to the sandwich construction of the skull bone, the test samples previously described have a variable structural geometry. These specimens contain the full cross section except they are ground flat on the top and bottom corresponding to the inside and outside of the skull. This results in a specimen with an inner and outer table of compact bone and a core of cancellous bone. The mechanical properties of compact bone are much more uniform and predictable than cancellous bone. The marrow spaces and trabecular arrangement of the diploë are highly variable, this giving rise to a wide range of mechanical responses. In order to ascribe meaningful material properties to this cancellous bone, one must have a correlation with the internal geometry. We are currently performing analysis of a variety of models to develop this correlation but with limited success. The limitation is the amount of geometrical detail that is practical to build into the model.

EXPERIMENTAL PROCEDURES

Density

The density of the specimens was determined by measuring the external dimensions of the specimen to determine the volume and by dividing this into the dry weight. After the mechanical properties tests are completed, the specimens were dried by baking at 105° until no further weight loss is observed. This density was therefore the weight of dry bone per unit volume and provides a convenient method of estimating the porosity.

Compression

Compression tests were performed on the type 'B' specimens of human bone and type 'C' specimens of monkey bone (McElhaney and Byars, 1966). The type 'B' specimens are loaded first in one direction to about $\frac{1}{3}$ the ultimate strength, while the deformation is measured in the direction of the load and also perpendicular to it. This is repeated in the other two directions yielding the stiffness and Poisson's ratio for the three axes, that is the radial and the two tangential to the head directions. The load is taken to failure in the third of these tests. Due to the thinness of monkey bone the type 'C' specimens are loaded in the tangential direction only.

The load was applied by a Tinius Olsen electromatic Testing Machine at a constant velocity of 0·01 in./min. The load was monitored by a very stiff strain gage type load ring while the deformation in the direction of the load and perpendicular to the load were measured with very compliant strain gaged cantilever contact arms (Fig. 4). These signals were continuously recorded on an $x-y_1-y_2$ recorder. The slope of these curves was used to compute the modulus and Poisson's ratio.

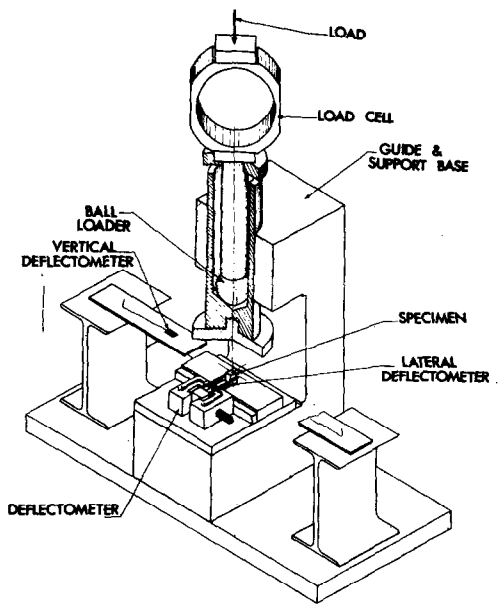

Fig. 4. Compression test apparatus.

The ultimate strength was the stress corresponding to the maximum load the specimen could withstand, generally characterized by a slope reversal. The ultimate strain was taken as the magnitude of the strain at the maximum load. The energy absorption capacity was determined as the work done on the material per unit volume in loading to the maximum load, and was proportional to the area under the load-deflection diagram.

Tension

Tension tests to failure were performed on miniature reduced section specimens. In some cases the total cross-section was tested, while in other cases the inner or outer table of compact bone was isolated and tested (see Wood 1969), for a complete description of this test). The load was applied by the above mentioned testing machine through specially designed grips supported on spherical bearings to minimize eccentricity. The load was monitored by a strain gage type load ring and the deformation was measured by a specially designed clip gage with a $\frac{1}{4}$-in. gage length or by strain gages cemented to the bone surface. The load deformation data was recorded on an $x-y$ plotter and appropriate properties determined as in the compression test.

Simple shear

A simple shear test was performed on type 'A' specimens by gripping the ends containing the inner and outer table in collets and moving one collet with respect to the other. A rigid guide was used to maintain the axes of the collets parallel (Fig. 5). Load and deformation were measured and recorded as in the compression test. With this arrangement, the diploë was loaded in simple shear. The collets were fixed $\frac{3}{16}$ in. apart resulting in a length to diameter ratio less than one. In addition, the collet assembly was supported in an indexing cylinder which allowed rotation as a unit of both cylinders and the specimens. Then the shear load could be applied in various directions. Each specimen was loaded to approximately $\frac{1}{3}$ the ultimate strength and the load-deflection curve recorded. The specimen was indexed 15° and loaded again. This procedure was continued until the specimen had been rotated 180° and the load axis then corresponded to the original one. Half the specimens were then rotated to the direction with the steepest slope and loaded to failure and the other half of the specimens were rotated to the direction with the lowest slope and loaded to failure. There was no significant difference in the ultimate strength in simple shear as determined from these two groups. The ratio of the largest to the smallest slope was a measure of isotropy for the specimen. For example, an aluminum specimen composed of 5 flat leaves was tested. When loaded parallel to the leaves, the slope of the load-deflection curve was 16 times larger than the slope when the load was applied perpendicular to the leaves. Since the surface tractions in this type of loading were unknown, the load-deflection diagrams could not be converted to stress or strain curves. By varying the load

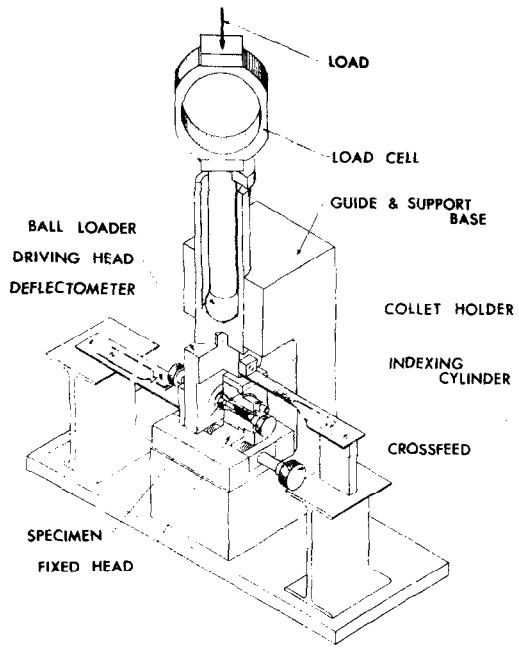

Fig. 5. Simple shear apparatus.

directions in the manner described above, a relative index of isotropy may be obtained. This index is the ratio of the largest slope to the smallest slope as obtained for a particular specimen.

Torsion

Collets similar to those described above were used to grip and twist type 'A' specimens. Specially designed torque and angle of twist transducers continuously monitored these quantities and an on-line $x-y$ plotter drew the torque-angle of twist curve. This curve was normalized to the shear stress–strain curve using the classical linear elastic homogeneous assumptions. The specimen was gripped in collets at both ends and torque applied about the cylinder axis. The inner and outer tables were constrained in collets and since they were much stiffer and stronger than the diploë this was essentially a test of the diploë with negligible influence from the compact bone of the tables.

In this test, as well as the other tests previously described, the assumption of classical elastic stress distributions was expedient but certainly not justified in the small. The short specimen lengths and obvious structural irregularities resulted in unknown stress variations. However, the assumed stress distributions were average values consistent with the statics of the loading situation. The material properties reported here are therefore reasonably representative of the bulk properties of skull bone.

Hardness

A microhardness test has been developed that allows the hardness of small regions (0·005 in. dia.) to be measured (Zeniya *et al.*, 1964). This test was performed on Tukon Microhardness Tester using a diamond pyramid indenter. The diameter of penetration under a 100/g load was converted to Vickers Hardness numbers. Four tests on the inner table surface and four tests on the outer table surface were made on each specimen.

RESULTS

A summary of the results of these tests is presented in Tables 1 and 2. The high values of the standard deviations are due to the naturally occurring variations of the diploë thickness and density. For human skull bone, no significant difference was found for the modulus and ultimate strength due to loading in various tangential directions. Histological studies of tangent sections of the inner and outer tables and the diploë, revealed random patterns without discernable geometrical organization. The index of isotropy, which is a quite sensitive measure of isotropy, was low and the maximum and minimum values of the modulus upon which it was based occurred in random directions. Thus, it was concluded that skull bone is reasonably isotropic in directions tangent to the skull surface.

There was no significant difference (90 per cent confidence level) between the microhardness tests for the inner and outer skull surfaces. In addition, there was no significant difference (90 per cent confidence level) between the microhardness tests for the human and monkey inner and outer tables. Since microhardness is a relative measure of combined strength-modulus properties, it may be concluded that there is little difference in these properties for the inner and outer surfaces of the skull. This conclusion agrees with the results of the tension tests on bone specimens from the inner or outer tables loaded in the tangent to the skull direction. No significant difference was observed for the tensile properties of bone from the inner and outer tables.

The fourth column of Tables 1 and 2 indicates the results of a student's t test comparing the mean value of the property for one skull with the mean value of all the tests. This was done in an attempt to determine whether the variation of the property within a single skull overshadowed the skull to skull variation. The results indicate that those properties related to diploë structure vary significantly skull to skull while those properties related more to material behavior do not.

Table 1. Properties of human cranial bone

Property	No. of specimens	No. of donors	Mean	Standard deviation	Skull to skull significant differences
Skull thickness in.	181	14	0·272	0·047	Yes
Diploë thickness in.	179	14	0·108	0·042	Yes
Dry weight density #/in^3	240	14	0·051	0·019	Yes
Modulus compression radial psi × 10^5	237	26	3·5	2·1	Yes
Secondary modulus compression radial psi × 10^5	65	11	0·53	0·4	No
Modulus compression tangential direction psi × 10^5	219	14	8·1	4·4	Yes
Poisson's ratio compression radial	122	14	0·19	0·08	No
Poisson's ratio compression tangential	327	18	0·22	0·11	No
Ultimate strength compression radial psi × 10^3	237	26	10·7	5·1	Yes
Ultimate strength compression tangential psi × 10^3	210	14	14	5·2	No
Ultimate strain compression radial in/in × 10^{-3}	237	26	97	80	No
Ultimate strain compression tangential in/in × 10^{-3}	210	14	51	32	No
Energy absorption compression radial in #/in^3	237	26	1200	700	Yes
Energy absorption compression tangential in #/in^3	189	14	480	440	No
Microhardness Vickers DPH inner table	181	14	31·6	9·3	No
Microhardness Vickers DPH outer table	181	14	34·2	8·0	No
Ultimate strength diploë direct shear psi × 10^3	348	17	3·1	0·5	No
Index of isotropy	52	8	2·5	1·2	No
Ultimate strength diploë torsion psi × 10^3	90	14	3·2	0·8	No
Modulus torsion diploë psi × 10^5	90	14	2·0	1·4	No
Ultimate strength tension tangential composite psi × 10^3	37	8	6·3	2·7	No
Modulus tension composite psi × 10^5	37	8	7·8	4·2	No
Ultimate strength tension tangential compact tables psi × 10^3	32	11	11·5	3·8	No

Table 1. (*cont.*)

Property	No. of specimens	No. of donors	Mean	Standard deviation	Skull to skull significant differences
Modulus tension compact tables psi × 10^5	32	11	1·78	0·3	No

Table 2. Physical properties of Rhesus monkey (*Macaca mulatta*) cranial bone

Property	No. of Specimens	Mean	Standard deviation	Skull to skull significant differences
Thickness in.	70	0·101	0·010	No
Dry weight density #/in^3	70	0·065	0·010	No
Ultimate strength compression tangential psi × 10^3	70	13·4	7	No
Modulus compression tangential psi × 10^5	70	9·4	4·6	No
Microhardness Vickers DPH inner table	70	32·4	12·2	No
Microhardness Vickers DPH outer table	70	34	10·2	No

Figure 6 presents typical stress–strain curves for human skull bone in compression. The modulus for tangential compression was generally more than 2X larger than for radial compression. Likewise, the ultimate strength was generally higher in the tangential direction than in the radial one. The ultimate strain and energy absorption capacity, however, were much larger for compression in the radial direction than the tangential direction.

Figure 7 shows three types of curves that were observed for radial compression. The upper curve is a classical compression curve and occurred in approximately 50 per cent of the tests. This type of curve indicates reasonably uniform stress with all parts of the specimen sharing the load. The middle curve shows progressive failure indicating that some trabeculae through the diploë layer were more highly loaded than others and failed or buckled prematurely. Since this type of curve was observed in approximately 25 per cent of the tests, the slope of the curve above the 'knee' is reported as a secondary modulus. The lower curve represents a test where the diploë was very porous and the trabeculae buckled throughout. Although this is a true response to compression load, the stress distribution is quite non-homogeneous and not comparable to the other types. For this reason, tests that indicated significant buckling were culled from the data and are not included in the tabulated results.

Figures 9 and 10 are maps of the diploë thickness and modulus (radial) of the human calvarium. These figures are three-dimensional displays drawn by computer and show graphically the variation of a measured property over a surface. In this case, the surface is developed from the projections of a grid on the calvarium.

Figures 11 and 12 show the variation of

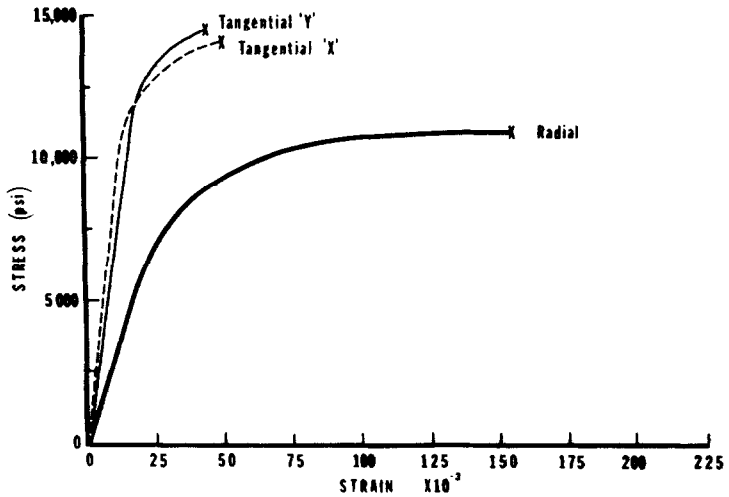

Fig. 6. Typical stress–strain curves for human skull bone in compression.

the compressive failure stress and modulus (radial) over the surface of the skull. This method of display contains much more detail but lacks the graphical impact of the computer plots. Fine grid maps of this type were examined in detail in an attempt to locate regions of weakness. It was observed that in general areas away from the sutures showed a much thicker diploë with a corresponding reduced radial compressive modulus and ultimate strength. However, the energy absorption capacity in these areas was higher. The problem of regions of weakness is therefore a complex and poorly defined one, requiring much more work for its solution.

Correlations with density

Regression analyses were performed to

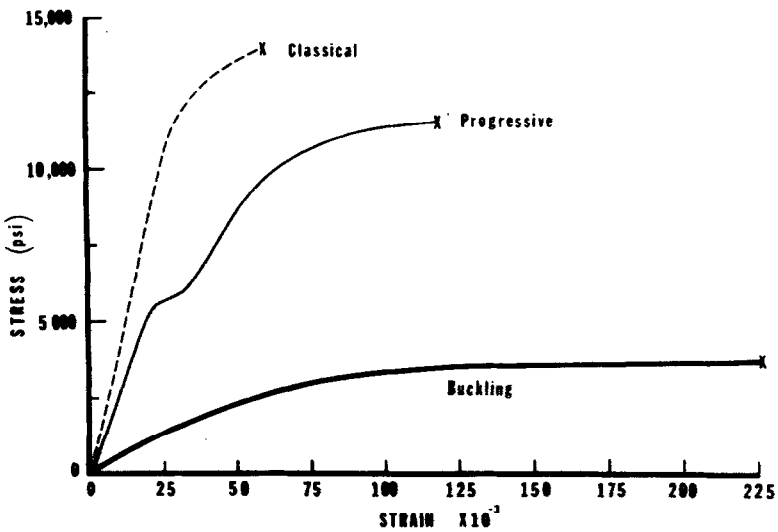

Fig. 7. Types of stress–strain curves for human skull bone in radial compression.

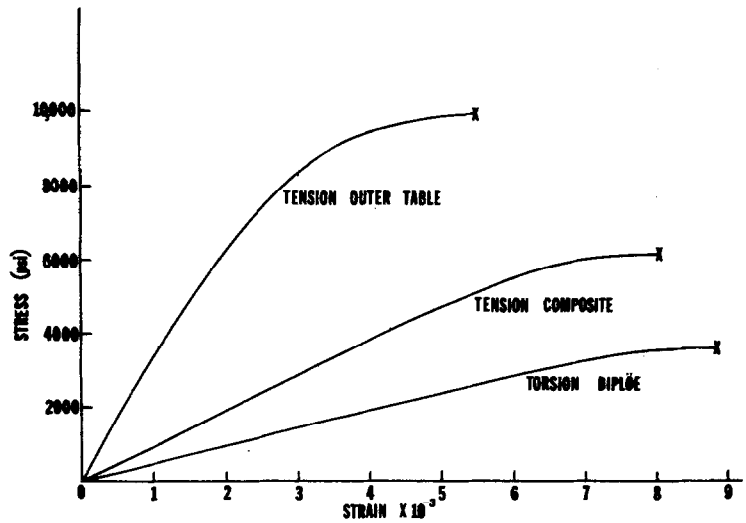

Fig. 8. Typical stress–strain curves for human skull bone.

correlate those properties that were anticipated to be functionally related. The following relationships were found for human cranial bone using data from those tests that produced classical stress–strain curves.

$$E_R = (2{\cdot}02 \times 10^{12}\gamma^{5{\cdot}13})\ \text{psi};\ C_c = 0{\cdot}86$$

$$\sigma = (2{\cdot}9 \times 10^{-2}\ E_R)\ \text{psi};\ C_c = 0{\cdot}78$$

$$\sigma = 1{\cdot}2 \times 10^{8}\gamma^{3{\cdot}3};\ C_c = 0{\cdot}91.$$

Radial compression

$$E_R = (36\gamma - 1{\cdot}3)\ \text{psi} \times 10^6;\ C_c = 0{\cdot}62$$

Tangential compression

$$E_t = (46\gamma - 1{\cdot}52)\ \text{psi} \times 10^6;\ C_c = 0{\cdot}65$$

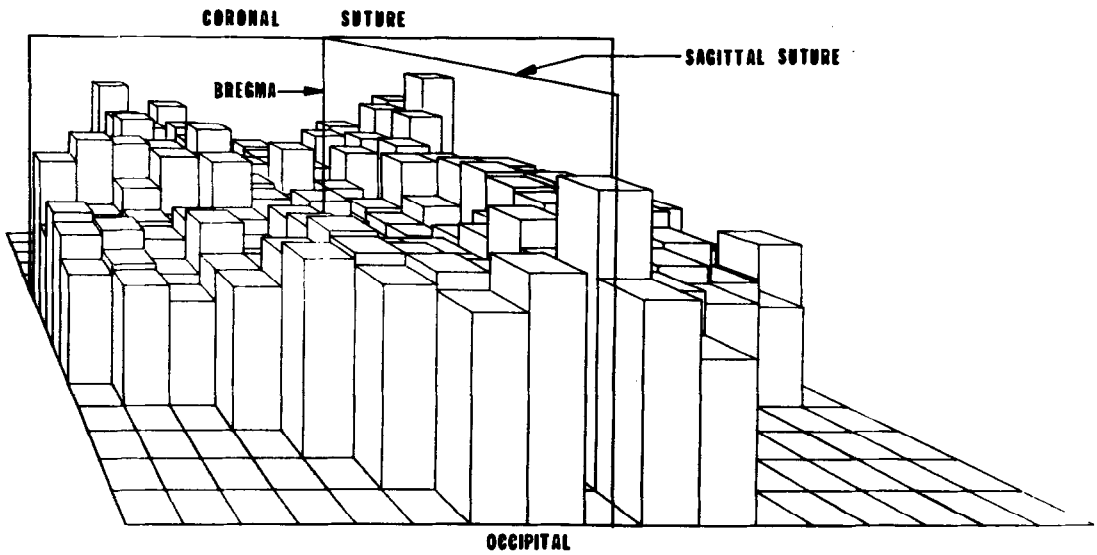

Fig. 9. Computer drawn presentation of diploë layer thickness.

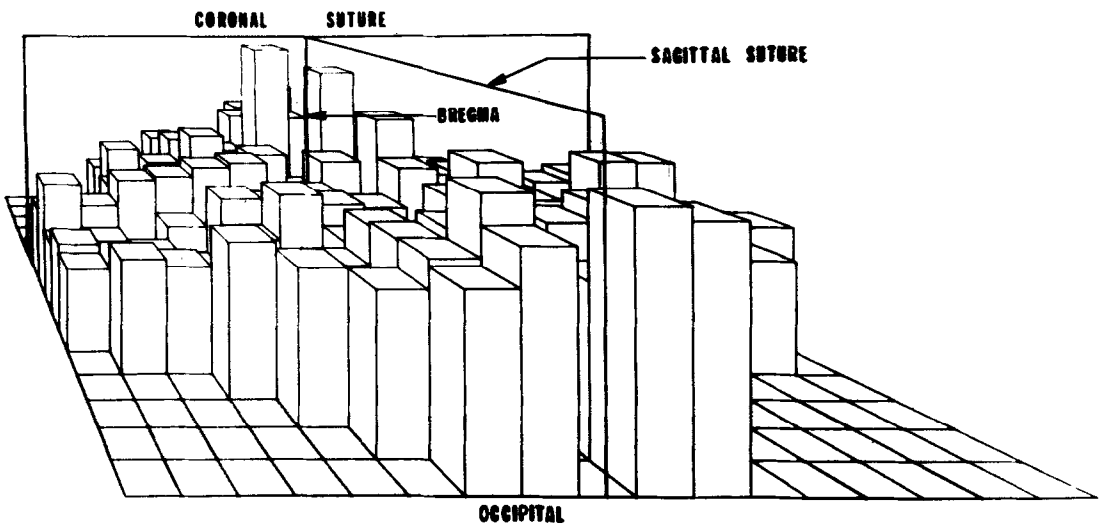

Fig. 10. Computer drawn presentation of compressive modulus of elasticity.

$$\sigma = (770\gamma - 26)\ \text{psi} \times 10^3;\ C_c = 0{\cdot}65$$

$$\sigma = 2{\cdot}4 \times 10^{-2}\, E_t\ \text{psi};\ C_c = 0{\cdot}57$$

where: E_R is the modulus of elasticity loaded in the radial direction (psi)
E_t is the modulus of elasticity loaded in the tangential direction (psi)
σ is the ultimate compressive strength (psi)
γ is the dry weight density (lb/in^3)
C_c is the correlation coefficient.

The values of the correlation coefficients indicate that a significant part of the variation in the modulus and strength may be attributed to variations in the density. The relation between density and modulus and density and strength was non-linear as evidenced by the higher values of the correlation coefficients or the logarithmic regression analysis compared with the linear regression analysis.

The relation between the stress and modulus was approximately linear however and indicated that the maximum strain may be taken as a constant value independent of porosity. This provided a basis for a maximum strain theory of failure for skull bone with failure strains of $2{\cdot}9 \times 10^{-2}$ for radial compression and $2{\cdot}4 \times 10^{-2}$ for tangential compression indicated by the regression analysis. It should be recognized, however, that these regression analyses were performed only on the data from the classical stress–strain curves, and those specimens that failed progressively or by buckling had much higher maximum strain values. The regression equations given are approximately valid for dry weight densities between 0·061 and 0·042 #/in^3 and should not be extrapolated beyond this range.

Porous block model

A physical ~ mathematical model has been developed that allows the prediction of the modulus and strength of bone based on its density and internal geometry (Alem, 1969). The accuracy of this prediction is limited by the natural variation of the properties of compact bone, the base material of the model. The advantage of such a model is that it allows the description, in a relatively compact form, of the physical properties of all types of bone, ranging from the dense bone of the femoral shaft to the very porous bone of the vertebral body (Currey, 1964; Stech, 1966). A model of

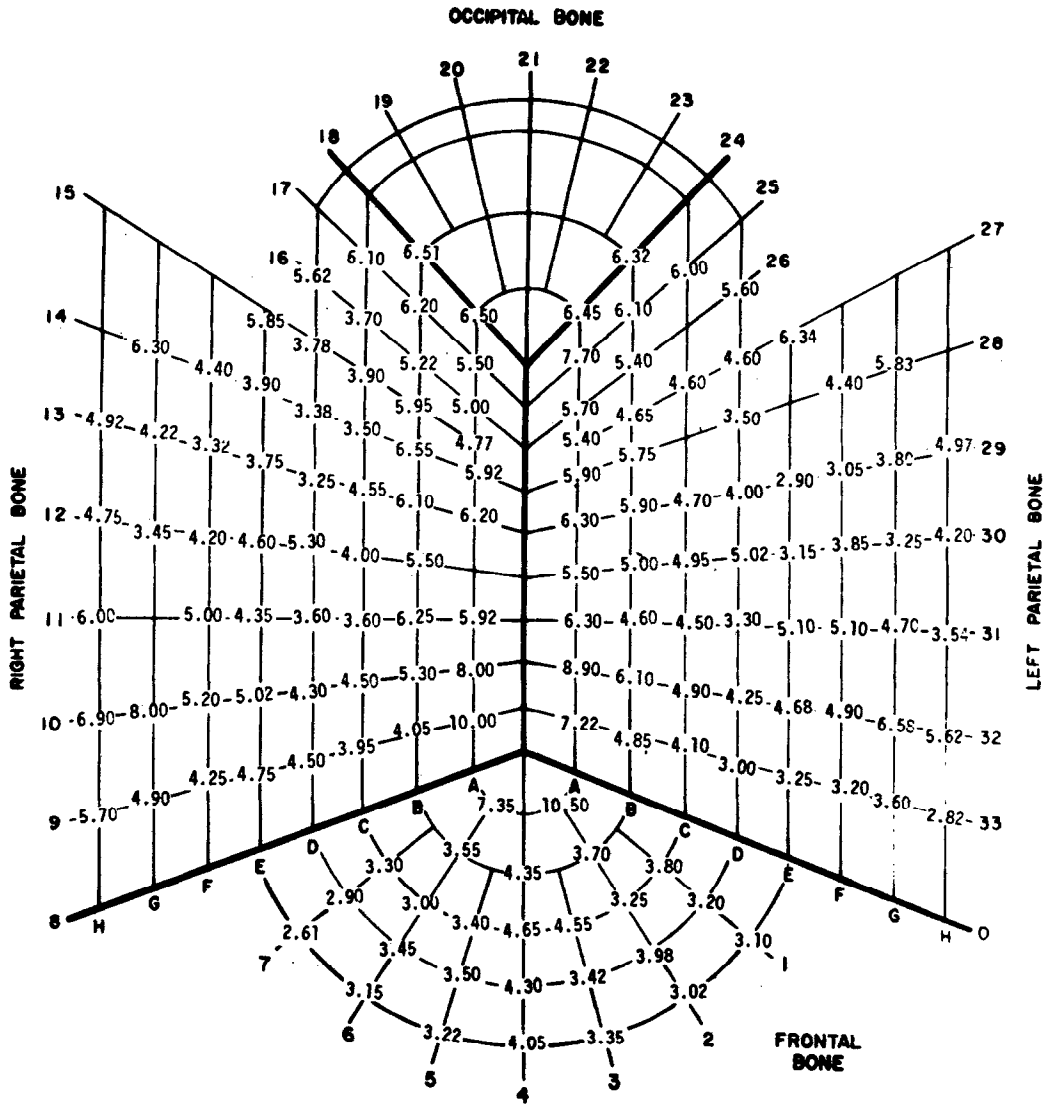

Fig. 11. Compressive failure stress.

this type may provide some insight into failure patterns and hopefully into treatment of multiple myeloma, osteoporosis and other diseases affecting the density of bone.

The primary assumption upon which this model is based is that all bone has the same physical properties in the small. That is, different types of bone have the same microscopic properties but varying microscopic structure. In dealing with the varying structure, it is further assumed that local mechanical responses like the modulus of elasticity and ultimate strength are proportional to the local density raised to some power (n).

Consider the porous block model shown in Fig. 13 which consists of a number of small cubical aggregates arranged to form a larger porous cube. In this model it is assumed that

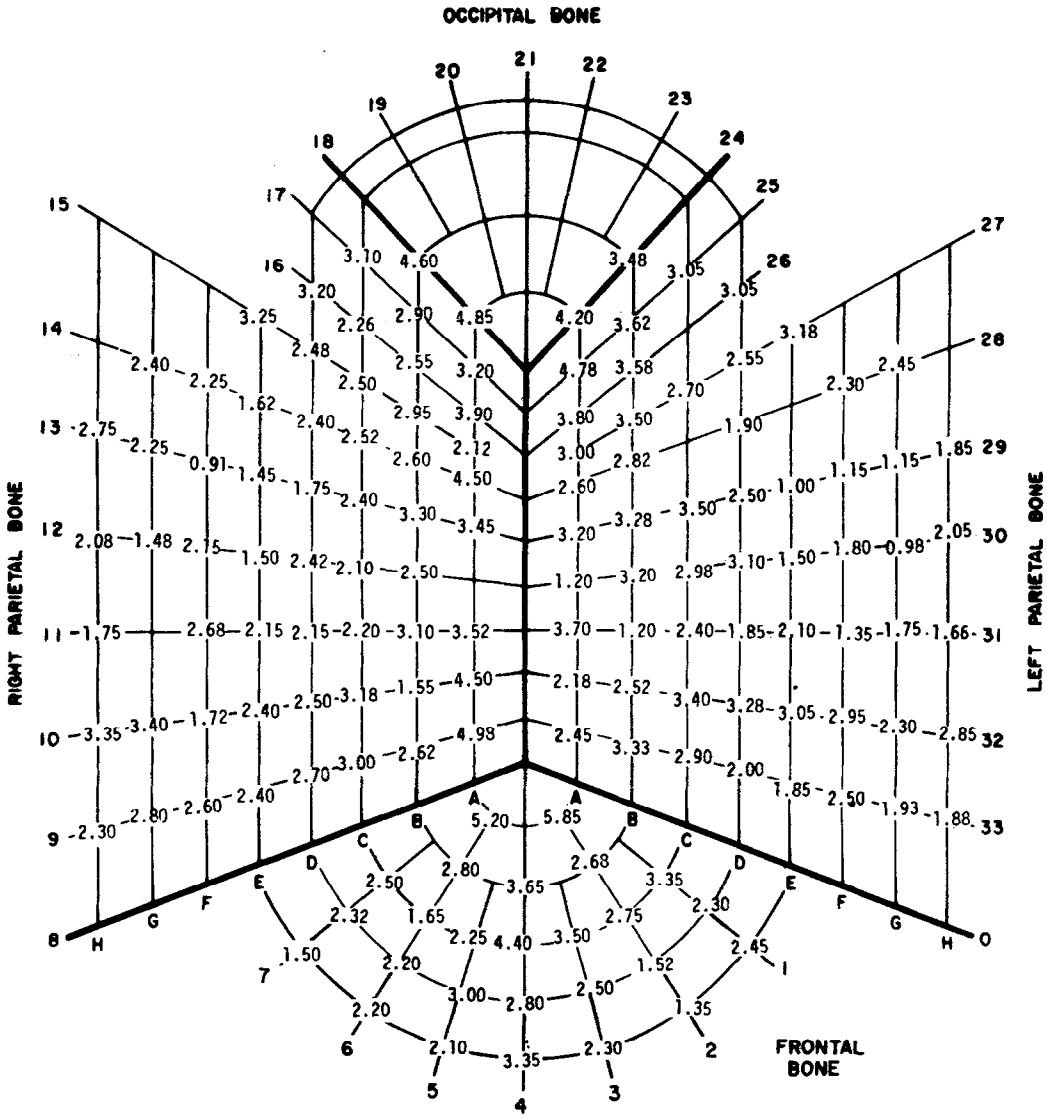

Fig. 12. Compressive modulus of elasticity.

the absence of one or more of the cubical aggregates from the large block does not alter either the position or the behavior of the neighboring aggregates. The ratio of the void volume to the total volume is called the porosity C,

thus

$$C = 1 - \gamma/\gamma_0$$

where γ is the density of the sample and γ_0 is the density of the base material.

A study of serial sections of cranial bone samples, conducted as part of the research program, has shown that the voids or marrow spaces are approximately homogeneously distributed in directions tangent to the inner and outer tables but in the radial direction there is a continuous increase in porosity as

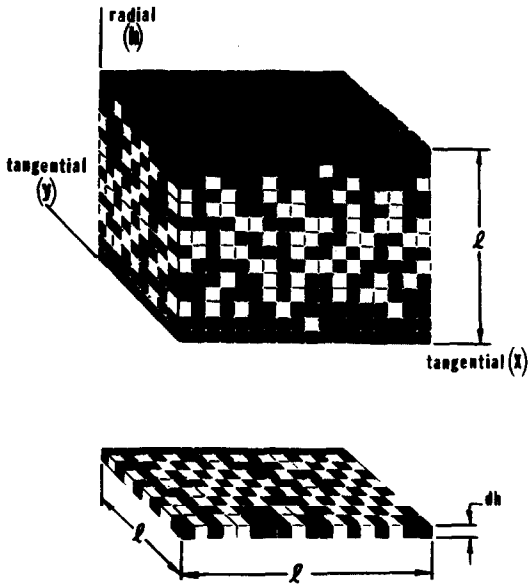

Fig. 13. Porous block model for cancellous bone.

one moves either from the inner or outer table toward the center. Thus, the model indicates that the modulus of elasticity of cranial bone samples loaded tangentially may be simulated by juxtaposition of a large number of slabs or springs loaded in parallel while radial loading is simulated by a large number of layers or springs loaded in series. Therefore,

$$\frac{E_0}{E_r} = \int_0^h \frac{dh}{[1-C(h)]^n} \text{ for radial compression, and}$$

$$\frac{E_t}{E_0} = \int_0^h [1-C(h)]^n dh \quad \text{for tangential compression,}$$

where E_0 is the modulus of the base material and $C(h)$ is the porosity of a slab or layer.

Additional study of serial sections of cranial bone indicated that the variation of porosity in the radial direction $C(h)$ could be satisfactorily approximated by a Gaussian function of the form

$$C_{(h)} = C_m{}^{-18\cdot42(h-1/2)^2}.$$

where C_m is the maximum porosity. With this form for $C_{(h)}$ the porosity of the tables is $C_m/100$.

The average porosity is then

$$C_a = \frac{1}{h}\int_0^h C_m e^{-18\cdot42(h-1/2)^2}\, dh.$$

It was found that for skewed distributions the modulus of the composite is independent of the location of C_m and no loss in generality is incurred by considering only symmetric distributions. These integrals do not possess closed form solutions but can be easily solved numerically on a digital computer.

Various values of the exponent n were examined by comparing the correlation coefficient relating the data to the model prediction. The value $n = 3$ was found to yield a best fit with a correlation coefficient of 0·79. In addition, several other porosity distributions were examined including parabolic and sinusoidal functions. The sinusoidal distribution did not give significantly different results from the Gaussian form presented here. Figures 14 and 15 show the relationship between modulus and porosity predicted by the model and compared with the regression analyses previously described.

The value of E_0, the modulus of the base material used to normalize the ordinate, was $1\cdot8 \times 10^6$ psi. This value was chosen to provide a best fit with the data and agrees well with the average value of 160 tension and compression tests of embalmed compact femoral bone ($1\cdot84 \times 10^6$ psi SD = $0\cdot41 \times 10^6$ psi) performed by the authors but as yet unreported, and with the 32 tension tests of predominately fresh compact bone from the inner and outer tables of the cranium ($1\cdot78 \times 10^6$ psi, SD = $0\cdot3 \times 10^6$ psi) reported here. The porosity was based on a value of 0·068 #/in^3 for the density γ_0 of compact bone which was the value determined from the above mentioned femoral and cranial specimens. The homogeneously distributed porosity version of this model agrees well with data for human vertebral bodies tests with porosities ranging to 65 per

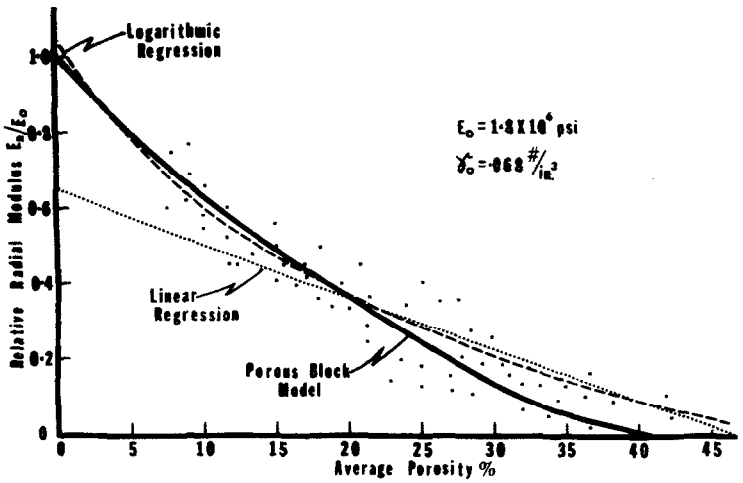

Fig. 14. Normalized radial modulus vs. porosity, human cranial bone in compression.

cent at one extreme and to data for femoral compacta tests with a porosity of 0 per cent (by definition) at the other.

The model indicates that with a Gaussian distribution of the form used here the average porosity cannot exceed 41 per cent because the maximum porosity at the center of the diploë can not be greater than 100 per cent. The value of the modulus is therefore much more sensitive to porosity distribution in the high porosity material than in the low porosity material.

Figure 16 shows the model's prediction of the ratio of the radial modulus to the tangential modulus compared with measured values. The model explains quite well the observed increase of non-isotropic response with increasing porosity. The non-isotropic mechanical response of the model is based on the non-isotropic porosity distribution and is very sensitive to the form of the porosity distribution in the region approaching 41 per cent average porosity. It is probable that much of the lack of fit in the low density region may be

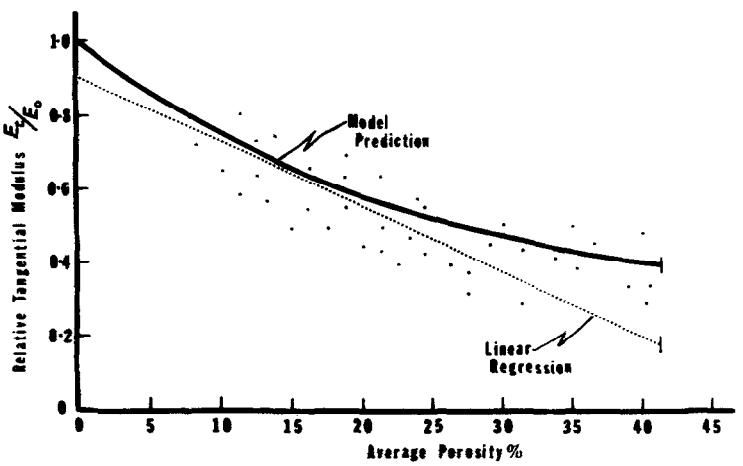

Fig. 15. Normalized tangential modulus vs. porosity, human cranial bone in compression.

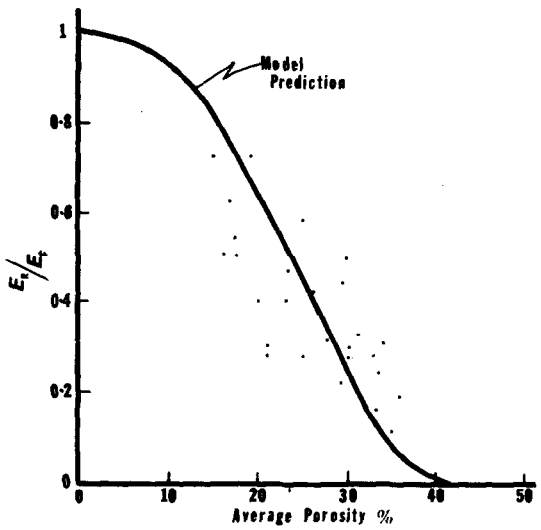

Fig. 16. Ratio of radial to tangential moduli vs. porosity.

explained by the difference between the actual porosity distribution in the sample and the assumed Gaussian distribution.

Figure 17 shows the response of the porous block model developed from the strength data. The ultimate strength of the base material was taken as 21,000 psi to obtain a best fit. This corresponds approximately to the long bone data, Evans (1957) and our own baseline experiments on compact femoral bone in compression (19,400 psi, SD = 6800 psi). In this figure the effect of porosity distribution is shown by comparing the Gaussian model prediction with the homogeneous model prediction. The value of the exponent used to obtain these model responses was 4 and the correlation coefficient comparing the model and the data was 0·67. In the low porosity range the Gaussian distribution yielded a satisfactory fit while in the high porosity range the homogeneous model gave better results.

DISCUSSION

Many of the mechanical responses of cranial bone are strongly influenced by the structural arrangement of the diploë (Endo, 1966, Gurdjian *et al.*, 1947). Thus in these tests properties such as compressive strength and modulus are structural properties and the large values of the standard deviations observed for these properties are primarily due to variations in the porosity and internal arrangement of the traebeculae. The microhardness tests and the tension test of the inner and outer tables indicate that a single material porous block model is justified as a first approximation in describing the relationship between structure and mechanical response. Relating the value of a property to the density raised to some power n and then determining n empirically provides a means of incorporating in the model many of the structural elements that influence the response but are too complex to

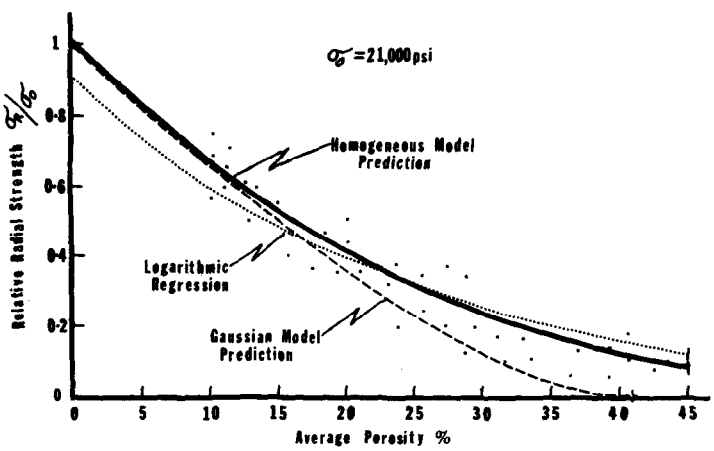

Fig. 17. Strength vs. porosity, human cranial bone in compression.

be included in detail. The model presented here is therefore complex enough to explain much of the property variation observed but much too simple to explain the mechanisms involved. The model shows that the modulus of bone is approximately proportional to the third power of the density and the strength is proportional to the fourth power of the density. Thus, small porosity changes in bone of low relative density result in only small changes in strength and modulus while small porosity changes in bone of high relative density result in large changes in strength and modulus. The porosity distribution in a given sample of bone is much more significant in its effect on strength and modulus in bone of low relative density than in bone of high relative density. Of interest is the fact that the homogeneous version of this model fits much of Coble's and Kingery (1956) data on various porous ceramics indicating that bone is not unique in its response to porosity variations.

The material properties in the small, i.e. hardness, density and local compression strength of human and primate (*Macaca mulatta*) cranial bone, are not significantly different. The amount and distribution of the diploë, however, is quite variable and therefore the structural responses—in particular the energy absorption, gross stiffness and damping characteristics which are strongly dependent on structure—will vary greatly.

Acknowledgements—The results reported in this paper represent a composite compilation of work performed in the Biomaterials Laboratory, H.S.R.I., The University of Michigan and the Biomechanics Laboratory, T.A.M., West Virginia University. Particular acknowledgement is given to the contributions of Jack Wood, Iqbal Barodawala, and Hurley Robbins from The University of Michigan, and Bruce Ours, Frank Ammons, George Utt and Richard Stalnaker from West Virginia University who performed much of the work presented here.

The research upon which this publication is based was performed pursuant to Contract No. PH43-67-1137 with the National Institutes of Health, National Institute of Neurological Diseases and Stroke, Public Health Service, Department of Health, Education and Welfare.

REFERENCES

Alem, N. M. (1969) A model for skull bone in compression. Master's Thesis, West Virginia University, Morgantown, West Virginia.

Coble, R. L. and Kingery, W. D. (1956) Effect of porosity on physical properties of sintered aluminea. *J. Am. ceramic Soc.* **29**, 377.

Currey, J. D. (1964) Three analogies to explain the mechanical properties of bone. *Biorheology* **2**, 1–10.

Dempster, W. T. (1967) Correlation of types of cortical grain structure with architectural features of the human skull. *Am. J. Anat.* **120**, 7–32.

Endo, B. (1966) A biomechanical study of the human facial skeleton by means of strain sensitive lacquer. *Okajimas Pol. Anat. Jap.* **42**, 205–217.

Evans, F. G. (1957) *Stress and Strain in Bones*. Thomas, Springfield, Illinois.

Evans, F. G. and Lissner, H. R. (1957) Tensile and compressive strength of human parietal bone. *J. appl. Physiol.* **10**, 492–497.

Evans, F. G. and Bang, S. (1967) Differences and relationships between the physical properties and the microscopic structure of human femoral, tibial and fibular cortical bone. *Am. J. Anat.* **120**, 79–88.

Gurdjian, E. S. and Lissner, H. R. (1947) Deformations of the skull in head injury as studied by the 'stresscoat' technique. *Am. J. Surg.* **73**, 269–281.

Gurdjian, E. S., Lissner, H. R. and Webster, J. E. (1947) The mechanism of production of linear skull fracture. *Surgery Gynec. Obstet.* **85**, 195–210.

McElhaney, J. H., Fogle, J., Byars, E. and Weaver, G. (1964) Effect of embalming on the mechanical properties of beef bone. *J. appl. Physiol.* **19-6**, 1234–1236.

McElhaney, J. H. and Byars, E. F. (1966) Dynamic response of bone and muscle tissue. *J. appl. Physiol.* **21**, 4.

Melvin, J. W., Robbins, D. H. and Roberts, V. L. (1969) The mechanical behavior of the diploë layer of the human skull in compression. *Dev. Mech.* **5**, 811–818.

Stech, E. L. (1966) A descriptive model of lamellar bone anisotropy. *ASME Paper* No. 66-HUF-3.

Wood, J. L. (1969) Mechanical properties of human cranial bone in tension. Ph.D. Dissertation, The University of Michigan, Ann Arbor, Michigan.

Zeniya, T., Takazono, K. and Ibuki, S. (1964) On the Vickers hardness of human temporal bone. *J. Kyoto Pref. Med. Univ.* **73**, 309–310 (Japanese text with English summary).

A Survey of Current Head Injury Research. A report prepared by the subcommittee on Head Injury, National Advisory Neurological Diseases and Stroke Council, National Institutes of Health, Bethesda, Maryland, 1969.